Bound-free spectra for diatomic molecules

David W. Schwenke

NASA Ames Research Center

M.S. T27B-1, P.O. Box 1000

Moffett Field, CA 94035-0001

It is now recognized that prediction of radiative heating of entering space craft requires explicit treatment of the radiation field from the infrared (IR) to the vacuum ultra violet (VUV). While at low temperatures and longer wavelengths, molecular radiation is well described by bound-bound transitions, in the short wavelength, high temperature regime, bound-free transitions can play an important role. In this work we describe first principles calculations we have carried out for bound-bound and bound-free transitions in N_2, O_2, C_2, CO, CN, NO, and N_2^+. Compared to bound-bound transitions, bound-free transitions have several particularities that make them different to deal with. These include more complicated line shapes and a dependence of emission intensity on both bound state diatomic and atomic concentrations.. These will be discussed in detail below.

The general procedure we used was the same for all species. The first step is to generate potential energy curves, transition moments, and coupling matrix elements by carrying out *ab initio* electronic structure calculations. These calculations are expensive, and thus approximations need to be made in order to make the calculations tractable. The only practical method we have to carry out these calculations is the internally contracted multi-reference configuration interaction (icMRCI) method as implemented in the program suite Molpro.[1] This is a widely used method for these kinds of calculations, and is capable of generating very accurate results. With this method, we must first of choose which electrons to correlate, the one-electron basis to use, and then how to generate the molecular orbitals.

In all calculations, we only correlate the valence electrons, *i.e.* the 1s-like orbitals are kept doubly occupied in all configurations. We initially considered correlating all electrons, which would yield more accurate results, however the extra expense was deemed un-warranted, given the difficulties with the icMRCI method for highly excited states. This will be discussed in more detail later.

For all calculations, the one-electron basis set used was based on the Dunning[2] cc-pVTZ basis set, which is the smallest one-electron basis set capable of yielding reasonable results. We also used the second order Douglas-Kroll-Hess[3] approximation to treat scalar special relativity. To help describe the outer-most electron clouds, the cc-pVTZ basis set was augmented by one extra diffuse function for each shell for C and N, and two extra diffuse functions for each shell for O. The extra shells on O are required due to the importance of O^- configurations.[4] Furthermore, systems expected to have low-lying Rydberg states (the neutrals, but not the cations) had an additional diffuse function added for each shell.

The molecular orbitals were generated using the following composite procedure. We first generated valance molecular orbitals by carrying out a series of complete active space (CAS) calculations starting at large internuclear separations (100 a_o for neutrals and 1000 a_o for ions) and working our way in to small inter-nuclear separations. We will use the symbol r for inter-nuclear separation. About 50

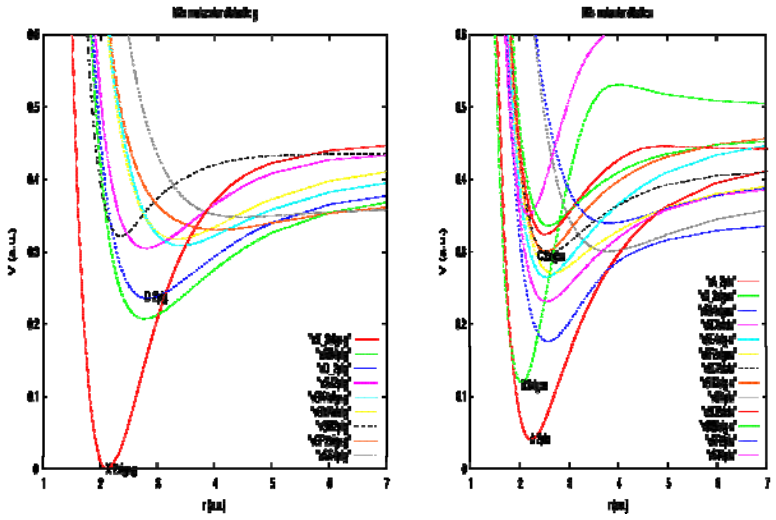

internuclear separations were considered. In these calculations, the O 2s-like orbitals were kept doubly occupied in all configurations. In the CAS calculations, several roots from each symmetry were optimized, with the weight for each root computed from the energy difference as described by Deskevich *et al.*[5] We based our selection of roots on the atomic states that we could reliable converge to. Thus our orbitals transform as $C_{\infty v}$ for heternuclear diatomics and $D_{\infty h}$ for homonuclear diatomics, and furthermore lead to the proper atomic degeneracies in the asymptotic region. We just considered a single overall electron spin: doublets for CN, N_2^+, CO^+, triplets for N_2, O_2, C_2, CO, and quartets for NO. For N_2, C_2, CO and NO. This choice of spin is not the same as the ground electronic state, but this choice gives better coverage of possible atomic states, thus it gives better overall results for all spins in the icMRCI calculations. The results from one internuclear separation were used as initial guess for the next smaller internuclear separation, and the *diab* procedure in Molpro was used to make the molecular orbitals, both active and virtual, look as similar as possible as the internuclear separation changed.

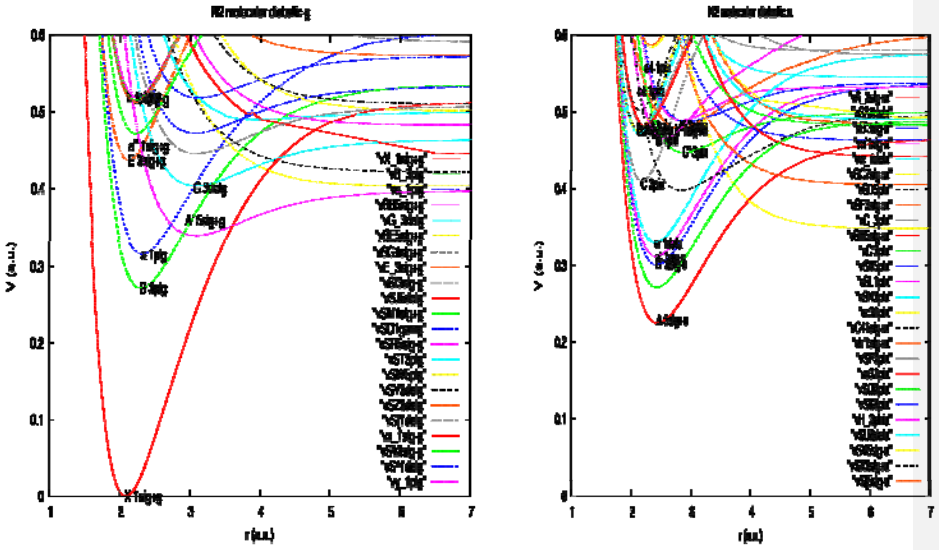

Once the valence molecular orbitals were determined, we determined low-lying Rydberg orbitals for the neutrals. For these calculations we started at the smallest inter-nuclear separations and worked our way to larger r values. The valence molecular orbitals were kept frozen at their previously determined values, and in the CAS calculations we restricted the configurations so that exactly one electron

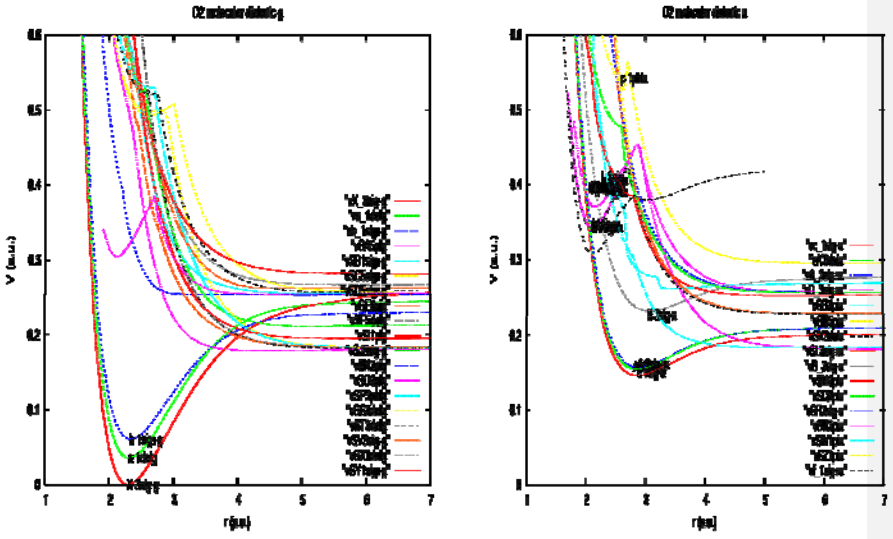

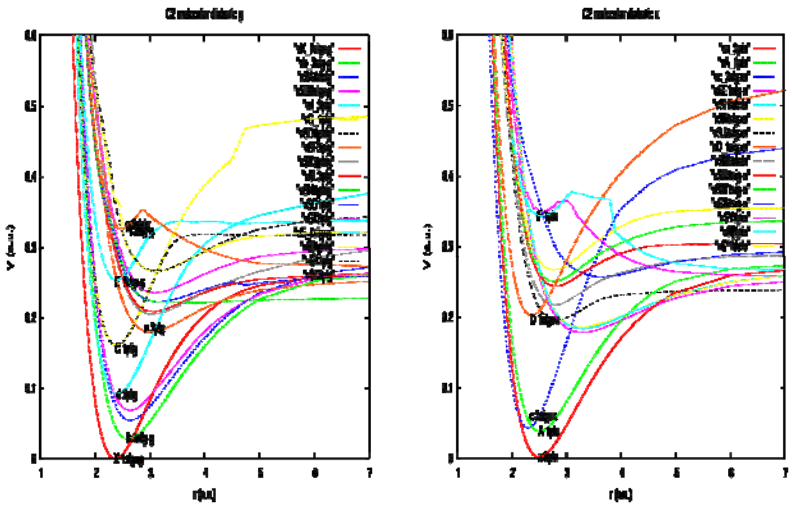

was kept in the Rydberg orbital of interest. For N_2, O_2, C_2, and CO, we used the lowest lying Rydberg singlet states, while for CN and NO we used the lowest lying Rydberg doublet states. In a sequential manner, we generated two σ Rydberg orbitals and both components of the π Rydberg orbital. As with the valence orbitals, we used the *diab* procedure in Molpro to ensure that the Rydberg orbitals smoothly changed with inter-nuclear distance.

Now we turn to evaluating the energies and coupling matrix elements. We carried

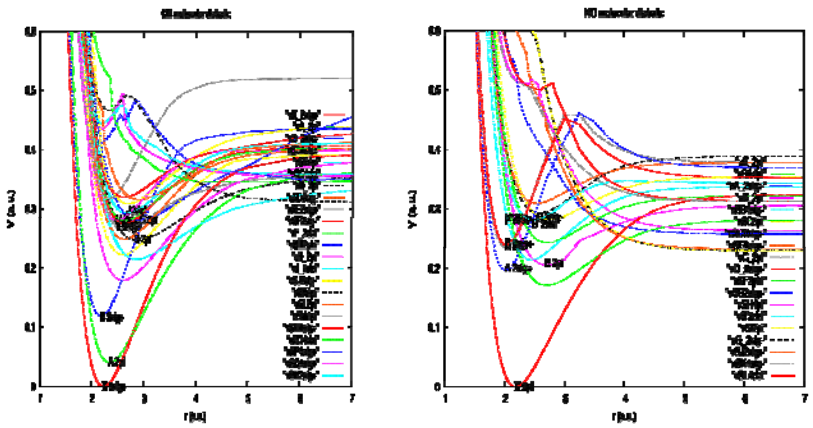

out icMRCI calculations for using an active space that consisted of all valence orbitals and all Rydberg orbitals: however O 2s valence orbitals where kept doubly occupied in the reference configurations and a maximum of one electron was allowed on the Rydberg orbitals. For these calculations, we used a modified version of Molpro that allowed the selection of Λ for the state of interest. Thus, Σ states were computed from separate icMRCI calculations then Δ states, etc. Nonetheless, it is necessary to extract multiple roots from the icMRCI calculations. These calculations can be carried out in two ways: the coupled state method, in which all roots are computed together and The projected state method, in which all roots are computed sequentially. The first approach is the default procedure in Molpro and has the advantages that the computed wave functions are orthogonal and have lower energies, and hence are more accurate, than the projected state energies. It has the disadvantage that the cost of calculation grows significantly as the number of states increases. Much more troublesome, however, is the fact that changes in the character of higher states can lead to discontinuous changes in lower state energies. The advantage of the projected state calculations is that the cost is linear in the number of roots, and state energies are continuous as the internuclear separation changes. The disadvantages of the projected state calculations are the electronic wave functions are no longer orthogonal and, if one is unlucky, a state flipping can occur that causes the calculations to fail. Thus neither method will always give reliable results. For the most part, we use the projected state method, with the coupled state method used selectively for O_2 and CO+. The unpleasant features that occasionally occur in high lying roots in the figures shown is mainly due to this problem.

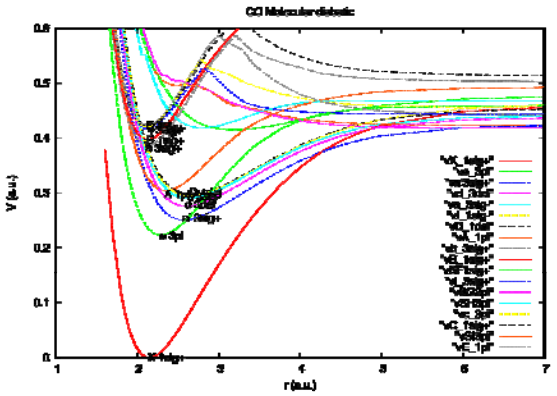

Using these electronic wave functions, we computed the energies, the overlaps, the dipole moment, the quadrapole moment, the magnetic dipole moment, and spin-orbit matrix elements for all possible couplings. Furthermore, to ascertain the relative phases of matrix elements and to transform from the adiabatic to a diabatic basis, we computed the overlaps of the wave functions from adjacent inter-nuclear separations.

Now let make a slight digression. The energies computed as described above are known as adiabatic energies, for the nuclei are "clamped" to fixed positions in the calculations of the electronic energies. However, for accurate calculations, it is

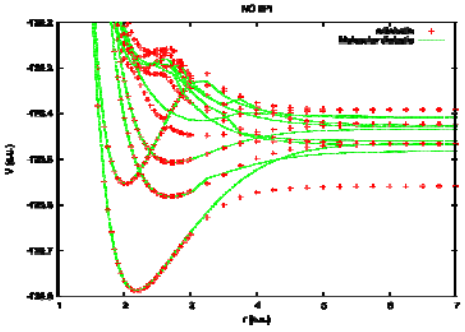

important to consider the effect of unclamping the nuclei on the electronic properties. This is most readily shown in the $^2\Pi$ manifold of NO: in the figure the symbols are the adiabatic energies, and the lines are Molecular diabatic energies. The adiabatic energies show numerous avoided crossings as the Rydberg state comes down in energy. At these crossings, the electronic wave function changes rapidly from one side to the other, and thus the coupling between the internuclear coordinate and the electronic wave functions will be very large. Even though this coupling can be included in the calculations in a fairly straightforward manner, other complications with using the adiabatic electronic functions remain. Namely the matrix elements of other operators, such as the dipole moment, have very complex behavior in the vicinity of an avoided crossing, which makes reliable interpolation difficult. It is thus advantageous to transform to a different electronic basis that does not have these problems because the character of the electronic wave functions has been forced to vary slowly and smoothly. This type of basis is called a diabatic basis. Several different choices for the diabatic basis are possible, and the particular basis we use we call the Molecular diabatic basis. This diabatic basis is formed recursively requiring that the adiabatic and diabatic basis be the same at the inter-nuclear separation where the adiabatic potential energy curve has its deepest minimum. In practice, we start with the internuclear separation at the lowest minimum, then propagate both forward and backwards in r. The propagation involves a series of Jacobi-type rotations, applied to the overlap between the electronic functions at neighboring geometries to make it as diagonal as possible. The Jacobi rotations are only applied to one side of the overlap matrix, and each individual rotation angle is chosen to minimize the off diagonal overlap of each pair of states. Sweeps through the matrix are carried out until the off diagonals of the matrix stop decreasing. In the diabatic basis, off-diagonal coupling due to electronic energy is non-zero, but all curves are smooth and easy to interpolate. The disadvantage of this basis is that convergence to the adiabatic atomic energies is rather slow in the asymptotic region. However this is not expected to be a critical part of predicting accurate molecular spectra.

Another thing to note about this figure is the diabatization procedure not only turns the sharply avoided crossings into real crossings, but also changes the large r-dependence of the ground state potential. In the large r region, the ground state potential does not exhibit any obvious avoided crossings, so that the diabatic curve differs from the adiabatic curve in this region might be surprising. However some consideration of the situation makes the situation more reasonable. In the large r region, the potential energy curves can be labeled by atomic quantum numbers, e.g. the lowest adiabatic potential curve has the asymptote of ^{3}P O + ^{4}S N. In the vicinity of the minimum, near r=2 a_o, the wave function will reflect a mixture of atomic states. For example, due to the higher electro-negativity of O over N, there will be significant O^- N^+ character in the wave function. In the Molecular diabatic states, the fractional character of the wave function is more or less frozen at its value at the minimum, thus the energy at the asymptote will be larger than the lowest adiabatic curve. This is exactly what we see. What happen to the ^{3}P O + ^{4}S N state in the molecular diabatic basis? After all, even in the vicinity of the minimum, the molecule is not purely O^-N^+. The O + N component should still be present. The NO figure appears to show a deficiency in the molecular diabatic basis. The loss of the ^{3}P O + ^{4}S N state would mean that one cannot use this basis for dissociation.

Name	Symmetry	Te calc	calc-obs	Name	Symmetry	Te calc	calc-obs
N2				C2			
A	3sig+u	49386	-817	a	3piu	470	-247
B	3pig	59690	70	b	3sig-g	6185	-249
B	3pig	59690	70	A	1piu	8487	96
B'	3sig-u	66051	-221	c	3sig+u	9544	-3768
a'	1sig-u	68493	340	d	3pig	20249	226
a	1pig	69480	197	C	1pig	35316	1054
w	1deiu	72367	270	D	1sig+u	44446	1207
G	3deig	88627	727	E	1sig+g	55695	660
C	3piu	89964	827	f	3sig-g	70287	-758
E	3sig+g	95972	114	F	1piu	74666	143
C'	3piu	98177	-174	N2+			
c3	1piu	104190	-286	A	2piu	8892	-275
C4	1sig+u	104457	-62	B	2sig+u	26100	638
b'	1sig+u	105155	657	D	2pig	51709	-610
o3	1piu	105871	2	CN			
H	3phiu	107392	1672	A	2pi	8885	-361
x	1sig-g	112843	-595	B	2sig+	26179	427
y	1pig	113816	-489	D	2pi	54101	-385
O2				F	2del	61325	1230
a	1deig	7790	-128	H	2pi	61479	-491
b	1sig+g	13279	84	J	2del	64185	-1074
c	1sig-u	32116	-941	CO			
A'	3deiu	33882	-808	E	1pi	93034	131
A	3sig+u	34474	-924	C	1sig+	92417	500
D	3sig+u	38868	-152	c	3pi	92157	-1002
B	3sig-u	50699	905	j	3sig+	91501	526
f	1sig+u	67375	-8716	B	1sig+	87246	301
e	1deiu	75410	156	b	3sig+	84871	1057
p	1phiu	119554	603	A	1pi	66714	1638
NO				D	1del	65431	-497
B	2pi	45239	-688	I	1sig-	64549	-536
A	2sig+	43306	-660	e	3sig-	63667	-563
C	2pi	51621	-505	d	3del	60574	-547
D	2sig+	52511	-574	a'	3sig+	55091	-734
B'	2del	61579	1215	a	3pi	48969	282
G	2sig-	64496	1583				

It is interesting to compare the computed potential energy curves with experimental data. In the figures, we have placed labels of electronic states at the value of T_e and r_e taken from Huber and Herzberg.[6] For the most part, the agreement is extremely good, graphically. The table above with the comparisons between the computed T_e and those given by Huber and Herzberg in wave numbers. While the differences are a small fraction of T_e, the absolute errors are sizable enough to be observed in say a spectrum from the EAST facility. Thus we shifted the curves for which data was available by the negative of the amount listed in the calc-obs columns. A more accurate procedure would be to use T_{00}, which is a more directly measured quantity, but the other approximations in the present work make this level of refinement superfluous.

Now it should be noted that this comparison and correction is not exact, for the values of T_e computed are just the differences in minimum energies in the Molecular diabatic curves, while the T_e from Huber and Herzberg is either the Y_{00} parameter in the Dunham expansion of the experimental energy levels for simple cases, or a parameter in a complicated effective Hamiltonian for more complex cases. Thus we

are comparing apples to oranges. Nonetheless it is expected that this correction will be reliable enough to yield useful results.

We next carried out coupled ro-vibrational-spin-electronic level calculations. To proceed we build up basis functions for all coordinates except the inter-nuclear separation:

$$\Psi^{JMP}_{\rho S\Lambda\Sigma} = \left[\frac{2J+1}{8\pi\left(1+\delta_{\Lambda 0}\delta_{\Sigma 0}\right)}\right]^{\frac{1}{2}} \left\{\Theta_{\rho S\Lambda\Sigma}(\tilde{\mathbf{x}})\mathscr{D}^{(J)}_{\Lambda+\Sigma M}(\phi\theta 0) + P\xi_{\rho}(-1)^{J+\tau}\Theta_{\rho S-\Lambda-\Sigma}(\tilde{\mathbf{x}})\mathscr{D}^{(J)}_{-\Lambda-\Sigma M}(\phi\theta 0)\right\}$$

with $P = \pm 1,\ \Lambda \geq 0$ and $\Sigma \geq 0$ when $\Lambda=0$. Here $\Theta_{\rho S\Lambda\Sigma}(\tilde{\mathbf{x}})$ is the spin-electronic function, with ρ labeling particular electronic states, S is the total electronic spin quantum number, Λ is the absolute value of quantum number specifying the projection of the total electronic angular momentum on the inter-nuclear bond axis, Σ is the quantum number specifying the projection of the total electronic spin angular momentum on the inter-nuclear bond axis, and $\tilde{\mathbf{x}}$ specify spin-electronic coordinates in the frame of reference having the body fixed z axis along the inter-nuclear bond, J and M are the quantum numbers for the total angular momentum and the projection of the total angular momentum on the space fixed z axis. The body fixed and space fixed axis are related by the rotation by the Euler angles $\phi\theta 0$, P is the parity and $\tau=N_e/2$, where N_e is the number of electrons. The factor ξ_{ρ} is -1 for Σ^- states, and +1 otherwise. The $\mathscr{D}$ are the Wigner rotation matrix elements as defined by Edmonds.[7]

In this basis, the full relativistic Hamiltonian operator is diagonal in *JMP*. The non-relativistic part of the Hamiltonian is also diagonal in *S*. If all off diagonal coupling matrix elements are neglected, then this would be what is called the Hund's case a basis. However, we do not make this approximation, and rather include all coupling terms. Thus we can accurately treat all possible Hund's cases as well as all intermediate cases.

The matrix elements of the nuclear rotational angular momentum contribution R(R+1) to the kinetic energy is given by

$$\left\langle JM\rho S\Lambda\Sigma P\middle|R(R+1)\middle|J'M'\rho'S'\Lambda'\Sigma'P'\right\rangle = \delta_{JJ'}\delta_{MM'}\delta_{SS'}\delta_{PP'}$$

$$\times\left[\begin{array}{l}
\delta_{\Lambda\Lambda'}\delta_{\Sigma\Sigma'}\left\{\delta_{\rho\rho'}\left[J(J+1)+S(S+1)-\Lambda^2-2\Sigma(\Sigma+\Lambda)\right]+\left\langle\rho\Lambda\middle|L_x^2+L_y^2\middle|\rho'\Lambda\right\rangle\right\} \\
-\delta_{\Lambda\Lambda'}\delta_{\Sigma\Sigma'\pm1}\delta_{\rho\rho'}\left\{\left[J(J+1)-(\Lambda+\Sigma)(\Lambda+\Sigma')\right]\left[S(S+1)-\Sigma\Sigma'\right]\left[1+\delta_{\Lambda 0}\left(\delta_{\Sigma 0}+\delta_{\Sigma' 0}\right)\right]\right\}^{\frac{1}{2}} \\
-\delta_{\Lambda\Lambda'\pm1}2\left\langle\rho\Lambda\middle|L_x\middle|\rho'\Lambda'\right\rangle\left(\begin{array}{l}
\delta_{\Sigma\Sigma'}\left\{\left[J(J+1)-(\Lambda+\Sigma)(\Lambda'+\Sigma)\right]\left[1+\delta_{\Sigma 0}\left(\delta_{\Lambda 0}+\delta_{\Lambda' 0}\right)\right]\right\}^{\frac{1}{2}} \\
-\delta_{\Sigma\Sigma'\mp1}\left\{\left[S(S+1)-\Sigma\Sigma'\right]\left[1+\delta_{\Lambda' 0}\delta_{\Sigma' 0}+\delta_{\Lambda 0}\delta_{\Sigma 0}\right]\right\}^{\frac{1}{2}} \\
+\xi_\rho\xi_{\rho'}P(-1)^{J+\tau}\left(\delta_{\Lambda 0}+\delta_{\Lambda' 0}\right)\left\{\begin{array}{l}
\delta_{\Sigma-\Sigma'}\left[J(J+1)+(\Lambda+\Sigma)(\Lambda'+\Sigma')\right]^{\frac{1}{2}} \\
-\delta_{\Sigma+1,-\Sigma'}\left[S(S+1)+\Sigma\Sigma'\right]^{\frac{1}{2}}
\end{array}\right\}
\end{array}\right) \\
-\delta_{|\Sigma|\frac{1}{2}}\xi_\rho P(-1)^{J+\frac{1}{2}}\left[\begin{array}{l}
\delta_{\Lambda\Lambda'}\delta_{\Lambda 0}\delta_{\Sigma\Sigma'}\delta_{\rho\rho'}\left(J+\frac{1}{2}\right)\left(S+\frac{1}{2}\right) \\
+\xi_{\rho'}\delta_{\Lambda\Lambda'\pm1}\left(\delta_{\Lambda 0}+\delta_{\Lambda' 0}\right)\delta_{\Sigma-\Sigma'}\left\langle\rho\Lambda\middle|L_x\middle|\rho'\Lambda'\right\rangle\left(J+\frac{1}{2}\right)
\end{array}\right]
\end{array}\right]$$

In this expression, we only neglect the $L_x^2+L_y^2$ term, for it is currently difficult to calculate, and furthermore only varies by a few cm^{-1} across the potential energy curve.

Besides the customary electric dipole transition moment, we will consider higher order moments. This is because the LBH a←X N_2 transition is dipole forbidden. The next order moments are the electric quadrapole moment and the magnetic dipole moment. In general, the transition matrix elements in this basis are given by

$$\left\langle JMP\rho S\Lambda\Sigma\left|\sum_m \hat{O}^{qt}_m \mathscr{D}^{(q)}_{mm'}\right|J'M'P'\rho'S'\Lambda'\Sigma'\right\rangle = (-1)^{\Lambda+\Sigma-M}\left[\frac{(2J+1)(2J'+1)}{(1+\delta_{\Lambda 0}\delta_{\Sigma 0})(1+\delta_{\Lambda' 0}\delta_{\Sigma' 0})}\right]^{\frac{1}{2}}\delta_{SS'}\delta_{\Sigma\Sigma'}\begin{pmatrix} J & q & J' \\ -M & m' & M'\end{pmatrix}$$

$$\times\frac{1+PP'\mathscr{P}^t(-1)^q}{2}$$

$$\times\left[\begin{pmatrix} J & q & J' \\ -\Lambda-\Sigma & \Lambda-\Lambda' & \Lambda'+\Sigma\end{pmatrix}\left\langle\rho S\Lambda\left|qt\Lambda'-\Lambda\right|\rho' S\Lambda'\right\rangle\right.$$

$$\left.+\delta_{\Sigma 0}P'\xi_{\rho'}(-1)^{J'}\begin{pmatrix} J & q & J' \\ -\Lambda & \Lambda+\Lambda' & -\Lambda'\end{pmatrix}\left\langle\rho S\Lambda\left|qt-\Lambda-\Lambda'\right|\rho' S-\Lambda'\right\rangle\right]$$

where $\begin{pmatrix} \cdot & \cdot & \cdot \\ \cdot & \cdot & \cdot\end{pmatrix}$ is a 3-j symbol. Now this factorizes into a term that contains all the *M* dependence and the rest:

$$\left\langle JMP\rho S\Lambda\Sigma\left|\sum_m \hat{O}^{qt}_m \mathscr{D}^{(q)}_{mm'}\right|J'M'P'\rho'S'\Lambda'\Sigma'\right\rangle = (-1)^{-M}\begin{pmatrix} J & q & J' \\ -M & m' & M'\end{pmatrix}F^{JPJ'P'qt}_{\rho S\Lambda\Sigma\rho' S'\Lambda'\Sigma'}$$

Now our final wave -functions will consist of linear combinations of the $\Psi^{JMP}_{\rho S\Lambda\Sigma}$ with fixed *JMP*, but this will not effect this factorization, but will change from the labels $\rho S\Lambda\Sigma$ to ν. Then the rate of stimulated emission (aka Einstein A coefficient) from electric dipole radiation is

$$\Gamma^{SE(e1)}_{n\to n'} = \frac{2\omega^3_{nn'}}{c^3\hbar(2J+1)}\left|F^{JPJ'P'(e1)}_{\nu\nu'}\right|^2\left[\sum_{MM'}\begin{pmatrix} J & 1 & J' \\ -M & 1 & M'\end{pmatrix}^2+\begin{pmatrix} J & 1 & J' \\ -M & -1 & M'\end{pmatrix}^2\right]$$

$$=\frac{4\omega^3_{nn'}}{3c^3\hbar(2J+1)}\left|F^{JPJ'P'(e1)}_{\nu\nu'}\right|^2$$

the rate of stimulated emission from magnetic dipole radiation is

$$\Gamma^{SE(m1)}_{n\to n'} = \frac{\omega^3_{nn'}}{8c^5\hbar(2J+1)}\left|F^{JPJ'P'(m1)}_{\nu\nu'}\right|^2\left[\sum_{MM'}\begin{pmatrix} J & 1 & J' \\ M & 1 & M'\end{pmatrix}^2+\begin{pmatrix} J & 1 & J' \\ M & -1 & M'\end{pmatrix}^2\right]$$

$$=\frac{\omega^3_{nn'}}{12c^5\hbar(2J+1)}\left|F^{JPJ'P'(m1)}_{\nu\nu'}\right|^2$$

and the rate of stimulated emission from electric quadrapole radiation is

$$\Gamma_{n\to n'}^{SE(e2)} = \frac{\omega_{nn'}^5}{4c^5\hbar(2J+1)}\left|F_{vv'}^{JPJ'P'(e2)}\right|^2\left[\sum_{MM'}\begin{pmatrix} J & 2 & J' \\ M & 1 & M' \end{pmatrix}^2 + \begin{pmatrix} J & 2 & J' \\ M & -1 & M' \end{pmatrix}^2\right]$$

$$= \frac{\omega_{nn'}^5}{10c^5\hbar(2J+1)}\left|F_{vv'}^{JPJ'P'(e2)}\right|^2$$

We see the following selection rules: for electric dipole radiation (e1), $P = -P'$ and $|J - J'| \le 1$, while for both magnetic dipole (m1) and electric quadrapole (e2) radiation we have $P = P'$, and additionally for e2, $|J - J'| = 2$ is possible. With all other things being approximately equal in atomic units, m1 is down from dipole allowed transitions by a factor of $1/c^2$, or about 10^{-4}. Compared to m1, e2 is down about by ω^2, which about another 10^{-4} in the infra-red region, but nearing unity in the VUV.

So far we have just discussed our treatment of the angular-electronic degrees of freedom. The radial degree of freedom, r, is treated using the finite difference boundary value method including full coupling. We perform calculations of each value of *J* and *P* (the radial wave functions are independent of the *M* quantum number) and we explicitly integrate the transition moments over the radial functions, thus we do note need Hönl-London factors or the r-centroid approximation. Furthermore, by fully including all coupling terms, we explicitly obtain nonzero lambda doubling splittings, spin-forbidden transitions, and all perturbations.

When solving for the radial functions, we have two situations to consider. In the first, for bound levels, the boundary conditions are homogenous as $r \to 0$ and as $r \to \infty$. In the second, the total energy is above the lowest dissociation limit, thus the large r boundary conditions are inhomogenous. This complicates things considerably.

For bound levels, the homogeneous boundary conditions make the solution of the radial functions a banded eigen-value problem. Thus the energies are fixed by the boundary conditions.

On the other hand, for un-bound, or free levels, the energy is a free parameter, and we must employ scattering theory to determine the wavefunction. Then large r boundary conditions take the form

$$f_{\eta\eta'}(\mathrm{r}) \sim k_\eta^{-\frac{1}{2}}\left\{\exp\left(-ik_\eta \mathrm{r}\right)\delta_{\eta\eta'} - \exp\left(ik_\eta \mathrm{r}\right)S_{\eta\eta'}\right\}$$

where η labels channels (channels are the various asymptotically diagonal basis functions), $k_\eta = \sqrt{2\mu\left(E-\varepsilon_\eta\right)}$, where μ is the reduced mass for radial motion, E is the kinetic energy of the relative motion of the free particles, ε_η is the threshold energy for channel η, and S is the scattering matrix, which is a complex symmetric matrix. For notational simplicity, we have suppressed the energy label from the radial function f and the scattering matrix. Now we do not know *a priori* the values of the scattering matrix, so in practical calculations we solve for the functions $\tilde{f}_{\eta\eta'}$ subject to the boundary conditions $\tilde{f}_{\eta\eta'}\left(\mathrm{r}_{bc}\right) = \delta_{\eta\eta'}$. We then analyze the large r behavior of the numerical results, and form linear combinations to satisfy the desired boundary conditions. It should be noted that the above expressions are only valid when k_η is real, i.e. $E>\varepsilon_\eta$. For other channels, the radial functions decay exponentially at large r.

Now for free states, how should we sample E? The obvious answer is to use a density of energies so that the scattering matrix can be reliably interpolated over. This requires knowledge of the formal behavior of the scattering matrix. There are poles in the scattering matrix at discrete complex energies $E = \mathscr{E}_n + i\Gamma_n/2$, where n is a counting index. While complex energies are not physically obtainable, these poles have important consequences on the real energy axis. Specifically, at energies "far" from $\mathscr{E}_n$, i.e. greater than about Γ_n away, the phase of the determinant of S decreases monatonically with increasing E, but near $\mathscr{E}_n$, the phase abruptly

increases by 2π like $2\tan^{-1}\left[\Gamma_n/2\left(\mathscr{E}_n - E\right)\right]$. Physically, these poles correspond to "almost" bound states with decay life time $\hbar/\Gamma_n$. Thus we need to concentrate our E sampling near the $\mathscr{E}_n$. But once again, we do not *a priori* know the $\mathscr{E}_n$.

We obtain estimates of the $\mathscr{E}_n$ by enclosing the system in a finite box, which turns all free states into bound states. Then we can determine energy eigen values, and the $\mathscr{E}_n$ will be nearby some of these eigen values. By evaluating the energy derivative of the phase of the scattering matrix, we can isolate the $\mathscr{E}_n$, and then do a refinement to determine better estimates of $\mathscr{E}_n$ and Γ_n.

It would seem that knowing $\mathscr{E}_n$ and Γ_n and the $f_{\eta\eta'}$, we would be in a position to compute bound-free transitions just like bound-bound transitions, but further reflection reveals additional details that must be addressed. First of all, how should the $f_{\eta\eta'}$ be "normalized"? This is not well determined, since they are not square integrable functions. Secondly, which of the η' should we chose to compute transition matrix elements? Another way to look at this last problem is $f_{\eta\eta'}$ represents incoming flux in channel η' and outgoing flux in all open channels. But the physical situation should have no incoming flux, since all the population would be generated by photon absorption.

Formatted: Lowered by 4 pt

The proper solution of this problem is to directly couple the radiation field to the nuclear problem using Green's functions. This leads to a driving term in the differential equations for the radial functions, and a solution that looks like

$$g_\eta^l(\mathrm{r}) \sim \left(\frac{2\pi\mu}{k_\eta}\right)^{\frac{1}{2}} M_\eta^l \exp\left(ik_\eta \mathrm{r}\right)$$

with *l* indexing the particular bound state for the transition. The amplitude M_η^l is complex and depends on energy. Note that these differential equations are no more difficult to solve than the scattering equations. Then one finds that if $\mathscr{E}_n$ corresponds

Formatted: Lowered by 4 pt

to a very nearly bound state, then in the limit of the coupling of the true bound state to the continuum becomes zero, then if E is near $\mathscr{E}_n$,

$$\sum_\eta \left|M_\eta^l\right|^2 = A_n^l \frac{\Gamma_n}{2\pi}\left[\left(E-\mathscr{E}_n\right)^2+\Gamma_n^2/4\right]^{-1}.$$

That is, the emissivity looks like an Einstein A modulated by a Lorentzian, and that the Einstein A can be computed via

$$A_n^l = \pi\sum_\eta \left|M_\eta^l\right|^2\Big|_{E=\mathscr{E}_n}.$$

However this simple result is not true in general. This is because the M_η^l are complex numbers, and thus various poles can cause constructive and destructive interference. See the following figure for an example:

In this figure, the red is $\sum_\eta \left|M_\eta^l\right|^2$, which clearly shows first derivative like features rather than Lorentzian features. The green is the result of convolution with the Doppler broadening. One sees that the broadening for these sharp features can result in much of the positive portion of the feature being eliminated. In our calculations, we find that this sort of situation is the rule rather than the exception. Thus it is not sufficient to just evaluate the amplitude M_η^l at the $\mathscr{E}_n$, but rather it is important to have more energies in order to nail down the energy dependence of the amplitude in order to perform the Doppler broadening calculation. These

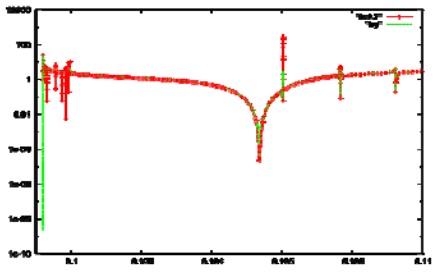

Formatted: Lowered by 4 pt

Formatted: Lowered by 4 pt

calculations are in progress, but have not yet been completed.

An additional complication is that in addition to emission from an almost bound state, there will be collision-induced emission at that energy. The emission from the almost bound state will be the product of the almost bound state population times $\sum_{\eta}\left|M_{\eta}^{l}\right|^{2}$. In contrast, the collision-induced emission will be the product of the atomic populations for channel η' times the factor $\sum_{\eta}\left|M_{\eta}^{l}-S_{\eta\eta'}\right|^{2}$. See below for an example. The red lines are for molecular emission while the other colors are for collision-induced emission.

Thus we only consider bound-bound transitions in this document. In the following figures, we show the optically thin absorption spectra of the diatomics computed at

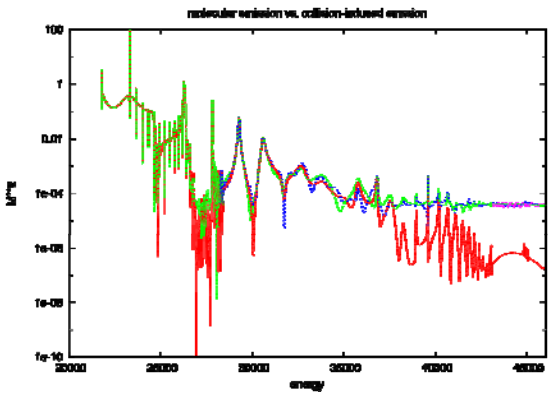

T=10,000K, which is roughly appropriate for Earth entry.

We see that in all cases except for N_2, the dipole transitions dominate the spectrum. We also see significant filling in of the spectra between peaks due to weak transitions, including spin-forbidden transitions.

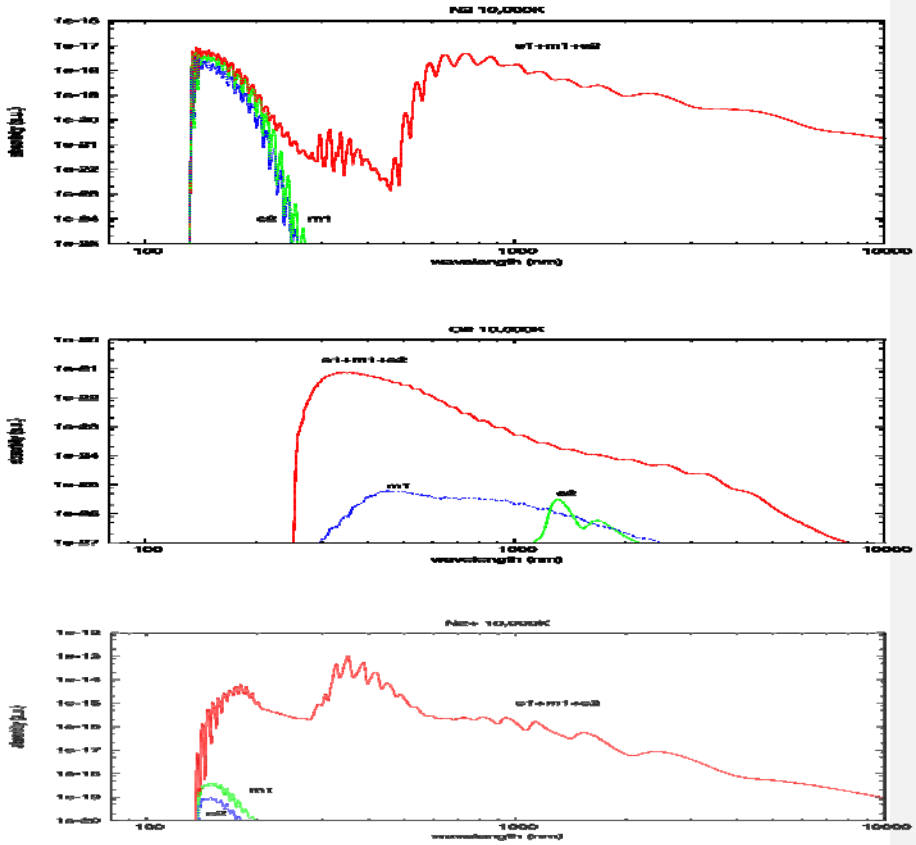
N2 10,000K
wavelength (nm)
O2 10,000K
wavelength (nm)
N2+ 10,000K
wavelength (nm)

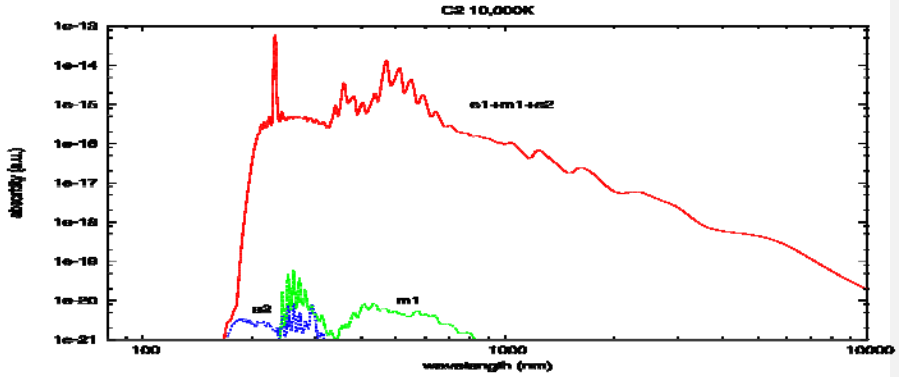
C2 10,000K
1e-13
1e-14
1e-15
1e-16
1e-17
1e-18
1e-19
1e-20
1e-21
100
1000
10000
wavelength (nm)
e1+m1+s2
m1
s2

References:

[1] MOLPRO is a package of ab initio programs written by H.-J. Werner, P. J. Knowles, G. Knizia, F. R. Manby, M. Schütz, P. Celani, T. Korona, R. Lindh, A. Mitrushenkov, G. Rauhut, K. R. Shamasundar, T. B. Adler, R. D. Amos, A. Bernhardsson, A. Berning, D. L. Cooper, M. J. O. Deegan, A. J. Dobbyn, F. Eckert, E. Goll, C. Hampel, A. Hesselmann, G. Hetzer, T. Hrenar, G. Jansen, C. Köppl, Y. Liu, A. W. Lloyd, R. A. Mata, A. J. May, S. J. McNicholas, W. Meyer, M. E. Mura, A. Nicklaß, D. P. O'Neill, P. Palmieri, K. Pflüger, R. Pitzer, M. Reiher, T. Shiozaki, H. Stoll, A. J. Stone, R. Tarroni, T. Thorsteinsson, M. Wang, A. Wolf .

[2] T.H. Dunning *J. Chem. Phys*. 90, 1007 (1989)

[3] M. Kouglas, N. M. Kroll, Ann. Phys. **82**, 89 (1974), B. A. Hess, Phys. Rev. A **32**, 756 (1985)

[4] D. W. Schwenke, Mol. Phys. 108 (19-20): 2751 (2010).

[5] M.P. Deskevich, D. J. Nesbitt, and H.-J. Werner, "Dynamically weighted multiconfiguration self-consistent field: Multistate calculations for $F+H_2O \rightarrow HF+OH$ reaction paths", J. Chem. Phys. Vol. 120, 2004, pp.7281

[6] K.-P. Huber and G. Herzberg, "Molecular Spectra and Molecular Structure: IV. Constants of Diatomic Molecules", Van Nostrand Reinhold, New York, 1979.

[7] D. Edmonds, "Angular Momentum", Princeton University Press, Princeton, 1962.